



## Highly doped InP as a low loss plasmonic material for mid-IR region

**Panah, Mohammad Esmail Aryaee; Takayama, Osamu; Morozov, S. V.; Kudryavtsev, K. E.; Semenova, Elizaveta; Lavrinenko, Andrei**

*Published in:*  
Optics Express

*Link to article, DOI:*  
[10.1364/OE.24.029077](https://doi.org/10.1364/OE.24.029077)

*Publication date:*  
2016

*Document Version*  
Publisher's PDF, also known as Version of record

[Link back to DTU Orbit](#)

*Citation (APA):*  
Panah, M. E. A., Takayama, O., Morozov, S. V., Kudryavtsev, K. E., Semenova, E., & Lavrinenko, A. (2016). Highly doped InP as a low loss plasmonic material for mid-IR region. *Optics Express*, 24(25), 29078-29089. DOI: 10.1364/OE.24.029077

## DTU Library

Technical Information Center of Denmark

---

### General rights

Copyright and moral rights for the publications made accessible in the public portal are retained by the authors and/or other copyright owners and it is a condition of accessing publications that users recognise and abide by the legal requirements associated with these rights.

- Users may download and print one copy of any publication from the public portal for the purpose of private study or research.
- You may not further distribute the material or use it for any profit-making activity or commercial gain
- You may freely distribute the URL identifying the publication in the public portal

If you believe that this document breaches copyright please contact us providing details, and we will remove access to the work immediately and investigate your claim.

# Highly doped InP as a low loss plasmonic material for mid-IR region

M. E. ARYAE PANAH,<sup>1,\*</sup> O. TAKAYAMA,<sup>1</sup> S. V. MOROZOV,<sup>2,3</sup> K. E. KUDRYAVTSEV,<sup>2,3</sup> E. S. SEMENOVA,<sup>1</sup> AND A. V. LAVRINENKO<sup>1</sup>

<sup>1</sup>Technical University of Denmark, Department of Photonics Engineering, Ørstedts Plads, Building 343, DK-2800 Kgs. Lyngby, Denmark

<sup>2</sup>Nizhniy Novgorod State University, 603950, 23 Gagarin Ave., Nizhniy Novgorod, Russia

<sup>3</sup>Institute for Physics of Microstructures, 603950, GSP-105, Nizhniy Novgorod, Russia

\*mesm@fotonik.dtu.dk

**Abstract:** We study plasmonic properties of highly doped InP in the mid-infrared (IR) range. InP was grown by metal-organic vapor phase epitaxy (MOVPE) with the growth conditions optimized to achieve high free electron concentrations by doping with silicon. The permittivity of the grown material was found by fitting the calculated infrared reflectance spectra to the measured ones. The retrieved permittivity was then used to simulate surface plasmon polaritons (SPPs) propagation on flat and structured surfaces, and the simulation results were verified in direct experiments. SPPs at the top and bottom interfaces of the grown epilayer were excited by the prism coupling. A high-index Ge hemispherical prism provides efficient coupling conditions of SPPs on flat surfaces and facilitates acquiring their dispersion diagrams. We observed diffraction into symmetry-prohibited diffraction orders stimulated by the excitation of surface plasmon-polaritons in a periodically structured epilayer. Characterization shows good agreement between the theory and experimental results and confirms that highly doped InP is an effective plasmonic material aiming it for applications in the mid-IR wavelength range.

© 2016 Optical Society of America

**OCIS codes:** (160.0160) Materials; (160.6000) Semiconductor materials; (050.1950) Diffraction gratings; (240.6680) Surface plasmons; (250.5403) Plasmonics.

## References and links

1. U. Fano, "The theory of anomalous diffraction gratings and of quasi-stationary waves on metallic surfaces (Sommerfeld's waves)," *J. Opt. Soc. Am.* **31**(3), 213–222 (1941).
2. S. A. Maier, *Plasmonics: Fundamentals and Applications* (Springer, 2007).
3. T. W. Ebbesen, H. J. Lezec, H. F. Ghaemi, T. Thio, and P. A. Wolff, "Extraordinary optical transmission through sub-wavelength hole arrays," *Nature* **391**(6668), 667–669 (1998).
4. J. A. Dionne, L. A. Sweatlock, H. A. Atwater, and A. Polman, "Planar metal plasmon waveguides: frequency-dependent dispersion, propagation, localization, and loss beyond the free electron model," *Phys. Rev. B* **72**(7), 075405 (2005).
5. D. J. Bergman and M. I. Stockman, "Surface plasmon amplification by stimulated emission of radiation: quantum generation of coherent surface plasmons in nanosystems," *Phys. Rev. Lett.* **90**(2), 027402 (2003).
6. H. A. Atwater and A. Polman, "Plasmonics for improved photovoltaic devices," *Nat. Mater.* **9**(3), 205–213 (2010).
7. J. B. Pendry, "Negative refraction makes a perfect lens," *Phys. Rev. Lett.* **85**(18), 3966–3969 (2000).
8. R. M. Ma, S. Ota, Y. Li, S. Yang, and X. Zhang, "Explosives detection in a lasing plasmon nanocavity," *Nat. Nanotechnol.* **9**(8), 600–604 (2014).
9. J. N. Anker, W. P. Hall, O. Lyandres, N. C. Shah, J. Zhao, and R. P. Van Duyne, "Biosensing with plasmonic nanosensors," *Nat. Mater.* **7**(6), 442–453 (2008).
10. J. Homola, "Surface plasmon resonance sensors for detection of chemical and biological species," *Chem. Rev.* **108**(2), 462–493 (2008).
11. S. Law, V. Podolskiy, and D. Wasserman, "Towards nano-scale photonics with micro-scale photons: The opportunities and challenges of mid-infrared plasmonics," *Nanophotonics* **2**(2), 103–130 (2013).
12. D. Rodrigo, O. Limaj, D. Janner, D. Etezadi, F. J. García de Abajo, V. Pruneri, and H. Altug, "Mid-infrared plasmonic biosensing with graphene," *Science* **349**(6244), 165–168 (2015).
13. A. N. Grigorenko, M. Polini, and K. S. Novoselov, "Graphene plasmonics," *Nat. Photonics* **6**(11), 749–758 (2012).

14. J. D. Caldwell, I. Vurgaftman, J. G. Tischler, O. J. Glembocki, J. C. Owrutsky, and T. L. Reinecke, "Atomic-scale photonic hybrids for mid-infrared and terahertz nanophotonics," *Nat. Nanotechnol.* **11**(1), 9–15 (2016).
15. A. Boltasseva, "Empowering plasmonics and metamaterials technology with new material platforms," *MRS Bull.* **39**(5), 461–468 (2014).
16. Y. Zhong, S. D. Malagari, T. Hamilton, and D. Wasserman, "Review of mid-infrared plasmonic materials," *J. Nanophotonics* **9**(1), 093791 (2015).
17. E. Sachet, C. T. Shelton, J. S. Harris, B. E. Gaddy, D. L. Irving, S. Curtarolo, B. F. Donovan, P. E. Hopkins, P. A. Sharma, A. L. Sharma, J. Ihlefeld, S. Franzen, and J. P. Maria, "Dysprosium-doped cadmium oxide as a gateway material for mid-infrared plasmonics," *Nat. Mater.* **14**(4), 414–420 (2015).
18. P. Biagioni, J. Frigerio, A. Samarelli, K. Gallacher, L. Baldassarre, E. Sakat, E. Calandrini, R. W. Millar, V. Giliberti, G. Isella, D. J. Paul, and M. Ortolani, "Group-IV midinfrared plasmonics," *J. Nanophotonics* **9**(1), 093789 (2015).
19. P. R. West, S. Ishii, G. V. Naik, N. K. Emani, V. M. Shalaev, and A. Boltasseva, "Searching for better plasmonic materials," *Laser Photonics Rev.* **4**(6), 795–808 (2010).
20. K. Anglin, T. Ribaudou, D. C. Adams, X. Qian, W. D. Goodhue, S. Dooley, E. A. Shaner, and D. Wasserman, "Voltage-controlled active mid-infrared plasmonic devices," *J. Appl. Phys.* **109**(12), 123103 (2011).
21. M. Shahzad, G. Medhi, R. E. Peale, W. R. Buchwald, J. W. Cleary, R. Soref, G. D. Boreman, and O. Edwards, "Infrared surface plasmons on heavily doped silicon," *J. Appl. Phys.* **110**(12), 123105 (2011).
22. J. C. Ginn, R. L. Jarecki, Jr., E. A. Shaner, and P. S. Davids, "Infrared plasmons on heavily-doped silicon," *J. Appl. Phys.* **110**(4), 043110 (2011).
23. W. Streyer, S. Law, G. Rooney, T. Jacobs, and D. Wasserman, "Strong absorption and selective emission from engineered metals with dielectric coatings," *Opt. Express* **21**(7), 9113–9122 (2013).
24. S. Law, L. Yu, A. Rosenberg, and D. Wasserman, "All-semiconductor plasmonic nanoantennas for infrared sensing," *Nano Lett.* **13**(9), 4569–4574 (2013).
25. Y. Zhong, P. B. Dongmo, L. Gong, S. Law, B. Chase, D. Wasserman, and J. M. O. Zide, "Degenerately doped InGaBiAs:Si as a highly conductive and transparent contact material in the infrared range," *Opt. Mater. Express* **3**(8), 1197–1204 (2013).
26. V. N'Tsame Guilengui, L. Cerutti, J. B. Rodriguez, E. Tournié, and T. Taliercio, "Localized surface plasmon resonances in highly doped semiconductors nanostructures," *Appl. Phys. Lett.* **101**(16), 161113 (2012).
27. M. Cada, D. Blazek, J. Pistora, K. Postava, and P. Siroky, "Theoretical and experimental study of plasmonic effects in heavily doped gallium arsenide and indium phosphide," *Opt. Mater. Express* **5**(2), 340–352 (2015).
28. Ch. Giesen, X. G. Xu, R. Hovel, M. Heuken, and K. Heime, "Silicon doping of InP grown by MOVPE using tertiarybutylphosphine," in *Proceedings of the International Conference on Indium Phosphide and Related Materials* (1997), pp. 47–50.
29. M. E. Aryaee Panah, S. Xiao, A. V. Lavrinenko, and E. S. Semenova, "Overcoming doping limits in MOVPE grown n-doped InP for plasmonic applications," in *16th European Workshop on Metalorganic Vapour Phase Epitaxy* (2015).
30. C. J. Gabriel and A. Nedoluha, "Transmittance and reflectance of systems of thin and thick layers," *Opt. Acta (Lond.)* **18**(6), 415–423 (1971).
31. W. H. Press, B. P. Flannery, S. A. Teukolsky, and W. T. Vetterling, *Numerical Recipes* (Cambridge University, 1986).
32. W. Walukiewicz, J. Lagowski, L. Jastrzebski, P. Rava, M. Lichtensteiger, C. H. Gatos, and H. C. Gatos, "Electron mobility and free-carrier absorption in InP; determination of the compensation ratio," *J. Appl. Phys.* **51**(5), 2659–2668 (1980).
33. S. Law, R. Liu, and D. Wasserman, "Doped semiconductors with band-edge plasma frequencies," *J. Vac. Sci. Technol. B* **32**(5), 052601 (2014).
34. S. Law, D. C. Adams, A. M. Taylor, and D. Wasserman, "Mid-infrared designer metals," *Opt. Express* **20**(11), 12155–12165 (2012).
35. G. V. Naik, V. M. Shalaev, and A. Boltasseva, "Alternative plasmonic materials: beyond gold and silver," *Adv. Mater.* **25**(24), 3264–3294 (2013).
36. I. J. Hodgkinson, S. Kassam, and Q. H. Wu, "Eigen-equations and compact algorithms for bulk and layered anisotropic optical media: reflection and refraction at a crystal-crystal interface," *J. Comput. Phys.* **133**(1), 75–83 (1997).
37. M. Sánchez-López, I. Moreno, and A. Martínez-García, "Teaching diffraction gratings by means of a phasor analysis," in *Proceedings of Education and Training in Optics and Photonics* (2009), pp. 1–12.
38. I. Epstein, I. Dolev, D. Bar-Lev, and A. Arie, "Plasmon-enhanced Bragg diffraction," *Phys. Rev. B* **86**(20), 205122 (2012).
39. I. Avrutsky, C. W. Smith, J. W. Cleary, and J. R. Hendrickson, "Resonant diffraction into symmetry-prohibited orders of metal gratings," *IEEE J. Quantum Electron.* **51**(12), 6600209 (2015).
40. A. S. Kuznetsov, P. Schäfer, W. John, D. Prasai, S. Sadofev, and S. Kalusniak, "Enabling novel functionality in heavily doped ZnO:Ga by nanostructuring: an efficient plasmonic refractive index sensor," *Nanotechnology* **27**(2), 02LT02 (2016).
41. COMSOL Multiphysics® v. 5.0. www.comsol.com. COMSOL AB, Stockholm, Sweden.

## 1. Introduction

Surface plasmon polaritons (SPPs) are surface waves confined to the interface between a dielectric and conductive materials as a result of coupling of an external electromagnetic field with the collective oscillation of free conduction electrons. Mathematical descriptions of these phenomena date back to early 1900's, but it was not until the middle of the 20th century when the experimental observations were linked to the theory [1]. Boosted by advances in nanofabrication techniques, the field of plasmonics was reborn in the second half of the 20th century [2]. Publication of Ebbesen *et al.* [3] in 1998 on extraordinary optical transmission propelled the interest to this field, and plasmonics quickly became one of the main research topics in nanophotonics due to broad potential applications. Unique properties of SPPs such as the subwavelength spatial confinement and high sensitivity of the dispersion to the surrounding dielectric material are exploited in subwavelength waveguides [4], surface plasmon lasers (spasers) [5], photovoltaics [6], optical superlenses [7] and plasmonic sensors [8].

Similar to the cases of visible and near-infrared regions, mid-IR plasmonics can contribute to many applications by means of intensely localized electric field at the interface and enhanced light-matter interactions. Plasmonics for the mid-IR wavelength region offers unique functionalities for thermal imaging, due to the peak emission wavelength for the temperatures ranging from 200 to 1400 K and the atmospheric transmission window both lying in the mid-IR. There are perspective chemo-sensing applications [9–12] owing to the fact that many molecules have vibrational and rotational absorption bands which can serve as fingerprints to detect and determine molecular species in this wavelength range. Moreover, the fast growing field of graphene plasmonics and related 2D materials operates in this wavelength regime as well [13, 14].

Traditionally noble metals are used as plasmonic materials due to their abundant free electrons in the conduction band. However, their large real and imaginary parts of the permittivity, especially in the infrared range, result in high loss and weak confinement to the surface. Apart from these material shortcomings, technological limitations pose an obstacle to integrating metals in conventional CMOS fabrication processes. During the last several years, alternative plasmonic materials such as conductive oxides, polar materials, graphene and doped semiconductors have become an emerging research field [11, 15–18]. Each group of alternatives has its own preferential wavelength range due to the available free carrier concentrations and mobilities. Semiconductors benefit from lower optical losses resulting from their high mobilities [19], drastic tunability of plasmonic properties via doping, the possibility of active control of the carrier concentration by charge depletion [20] and full CMOS compatibility. In this regard doped Si [21, 22], Ge [23], InAs:Si [24], InGaAsBi:Si [25] and InAsSb:Si [26] have been challenged for plasmonic properties.

InP as a direct bandgap III-V semiconductor is one of the most common materials in optoelectronic applications which has the advantages of easy integration and being compatible with conventional III-V optoelectronic devices and their fabrication processes. The InP based material system is conventionally used for telecom applications at 1300 and 1550 nm wavelengths. However, in spite of being the workhorse of the telecom photonics, literature on plasmonic properties of InP is scarce. Very recently, Cada *et al.* have used Fourier transform infrared (FTIR) spectroscopy together with Raman scattering measurements to determine the plasma frequency of heavily doped InP [27]. However, to the best of authors' knowledge, a rigorous analysis of the plasmonic properties of doped InP including the growth conditions, permittivity function restoration, characterization and direct experimental observation of SPPs has not been presented in the literature. This constitutes the goal of our publication.

## 2. Growth and dielectric function of highly doped InP

### 2.1 Growth

Two samples with 3  $\mu\text{m}$  and 400 nm thick InP:Si epilayers were grown using different growth conditions on single-side polished (1 0 0) InP:S substrates by low pressure MOVPE. The precursors for phosphorus, indium and silicon were phosphine ( $\text{PH}_3$ ), trimethylindium (TMIn) and disilane ( $\text{Si}_2\text{H}_6$ ) respectively. The growth conditions, namely the substrate temperature, phosphorus to indium precursors' molar ratio and the disilane flux were optimized resulting in the high free carrier concentration.

At low growth temperatures the carrier concentration is limited by the decomposition efficiency of disilane, which is exponentially dependent on temperature, therefore increasing the temperature results in higher carrier concentrations up to around 610°C. Above this temperature nearly all disilane molecules are dissociated, and the resulting carrier concentration becomes independent of the substrate temperature. The electron concentration is known to have a very slight proportionality with  $\text{PH}_3$  to TMIn molar ratio (V/III ratio) especially in temperatures higher than 610°C [28]. Increasing the disilane flux increases the electron concentration up to the threshold point, above which silicon clusters start forming on top of the sample leading to a rough surface [29].

Considering the above-mentioned conditions, the growth was carried out at an overall chamber pressure of 60 Torr for both samples with growth conditions summarized in Table 1. The resulting free electron concentrations in the grown epilayers measured by electrochemical capacitance-voltage (ECV) profilometry are given in the last column. The free electron concentration of the substrates of sample 1 and sample 2 are also measured to be  $5.4 \times 10^{18} \text{ cm}^{-3}$  and  $1.5 \times 10^{18} \text{ cm}^{-3}$  respectively.

**Table 1. Optimized growth conditions of the samples**

Sample No.	Growth temperature [°C]	V/III ratio	Disilane flux [SCCM]	Free carrier concentration [ $\text{cm}^{-3}$ ]
1	610	142	90	$3.15 \times 10^{19}$
2	610	125	50	$2.7 \times 10^{19}$

### 2.2 Dielectric function

The dielectric function of a material is the key to understand its optical and in particular plasmonic features. In this subsection we present the experimentally determined dielectric function of the grown highly doped InP. Further on, it is used to simulate excitation of SPPs on the surface of the samples.

The normal-incidence reflection spectrum for the epilayer-substrate system was calculated theoretically using the intensity transfer matrix method [30]. The purpose of this method is to get rid of the Fabry-Perot interference fringes from the 350  $\mu\text{m}$  thick substrate while retaining the fringes originated from the epilayer. In this way, theoretically calculated reflectance spectra will resemble the experimental ones, in which fringes from the substrate will be negligibly weak mainly due to the deviations from ideal conditions such as the rough back side of the wafer, etc. The Drude-Lorentz (D-L) dielectric function was used for analytical description of the InP permittivity. The Drude term typically accounts for the free electrons contribution to the optical response, and Lorentzians account for the contribution of phonons:

$$\varepsilon(\omega) = \varepsilon_{\infty} \left( 1 - \frac{\omega_p^2}{\omega^2 + i\omega\gamma} \right) + \sum_j \frac{S_j \omega_{f,j}^2}{\omega_{f,j}^2 - \omega^2 - i\omega\Gamma_j}. \quad (1)$$

Here  $\varepsilon_{\infty}$ ,  $\omega_p$ ,  $\gamma$  and  $i$  are the high-frequency dielectric constant, plasma frequency, electrons plasma damping and the imaginary unit ( $\sqrt{-1}$ ) respectively.  $S_j$ ,  $\omega_{f,j}$  and  $\Gamma_j$  are the

strength, resonance frequency and damping for the  $j^{\text{th}}$  Lorentzian oscillator respectively, describing a phonon absorption at frequency  $\omega_{f,j}$ .

Reflection from both the substrate wafers and the grown samples was measured for a near-normal angle of incidence ( $12^\circ$ ) between  $3 \mu\text{m}$  and  $40 \mu\text{m}$  wavelengths using VERTEX 70 FTIR spectrometer from Bruker. The spectra were normalized to the reflection from the aluminum mirror of the spectrometer's sample holder. The measurements were carried out at five different points of the samples in order to get statistically supported results.

Afterwards the calculated reflection spectra of the substrates were fitted to the experimental data in order to find the parameters of the D-L dielectric functions for the substrates. The fitting was done using the Levenberg-Marquardt algorithm [31], weighted with the inverse of the standard error for each measured point. These parameters were taken into account to fit the dielectric function parameters for the grown epilayers (Table 2). In all cases  $\epsilon_\infty$  is considered to have a constant value equal to 9.55 [32].

**Table 2. Fitted parameters of the D-L dielectric function**

Sample No.	$S_1$	$\Gamma_j$ [THz]	$\omega_{f,j}$ [THz]	$\gamma$ [THz]	$\omega_p$ [THz]
1 (epilayer)	3.83	0.036	9.13	2.76	39.27
1 (substrate)	2.62	0.05	9.09	2.17	17.3
2 (epilayer)	1.91	0.048	9.09	2.82	40.47
2 (substrate)	2.8	0.01	9.15	2.16	11.49

Figure 1 shows the reflectance spectra of the grown samples and bare substrates. As it can be seen from the figure, in case of highly doped InP, only one Lorentzian term is pronounced and others are overshadowed by the plasma resonance. Based on the retrieved parameters of the D-L model and Eq. (1), we plotted in Fig. 2 the complex permittivity and refractive index of samples 1, 2 and their substrates. The low doped InP (sample 2 substrate) becomes plasmonic at the wavelength  $\lambda_p = 22.7 \mu\text{m}$  as its permittivity turns negative [Fig. 2(a)]. The crossover wavelength of highly doped InP (sample 2 epilayer) can be shifted to the shorter wavelength  $\lambda_p = 7.4 \mu\text{m}$ , demonstrating the range for possible tuning of plasmonic properties through the carrier concentration control.

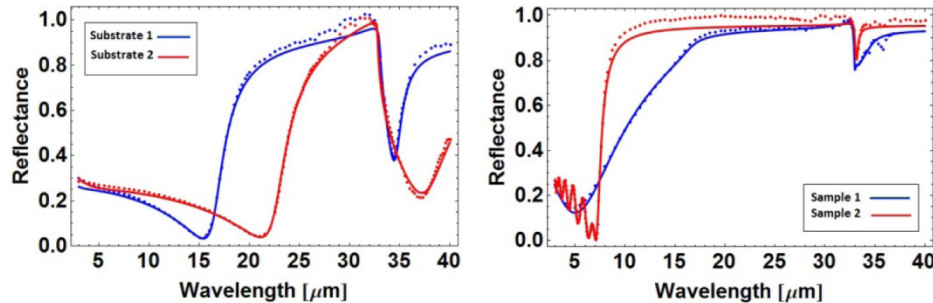


Fig. 1. Measured (dotted) and fitted (solid) reflectance spectra from bare substrates (left) and grown samples (right).

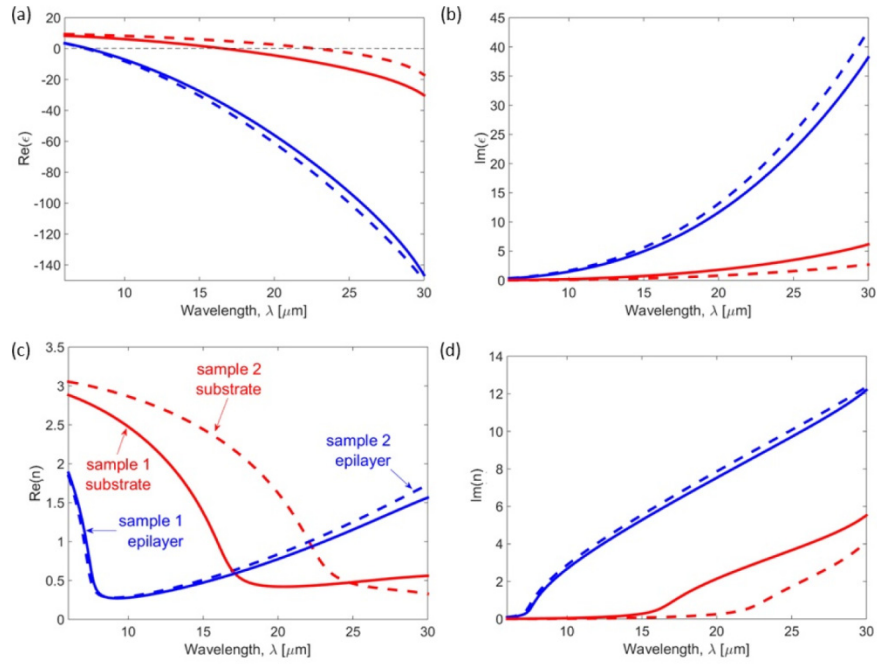


Fig. 2. (a) Real and (b) imaginary parts of the permittivities, (c) real and (d) imaginary parts of refractive indices of sample 1 (blue solid lines), 2 (blue dashed lines), substrate of the sample 1 (red solid lines) and the substrate of the sample 2 (red dashed lines) from Table 2.

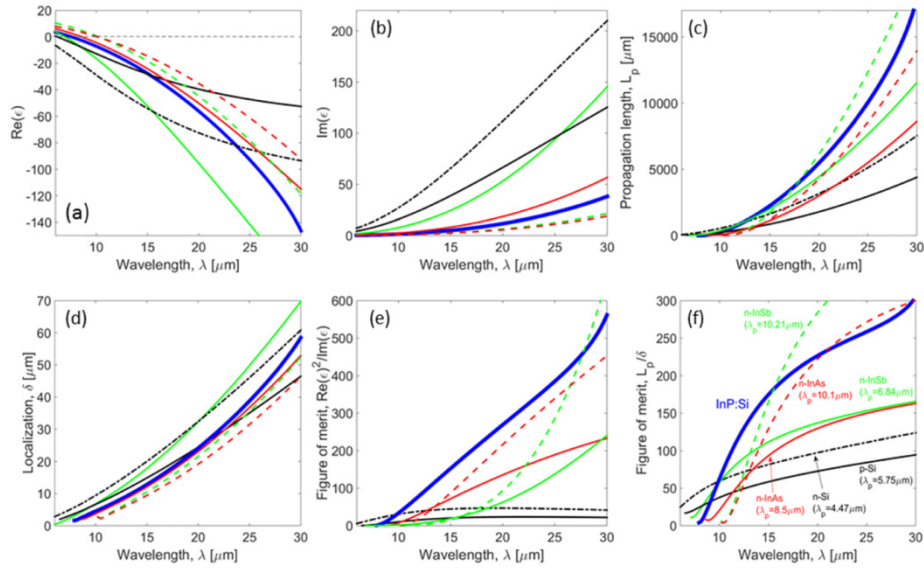


Fig. 3. (a) Real and (b) imaginary part of the permittivities of InP:Si (sample 1) from Table 2 as well as n- ( $\lambda_p = 4.47 \mu\text{m}$ ) and p-doped Si ( $\lambda_p = 5.75 \mu\text{m}$ ) [22], n-InSb ( $\lambda_p = 6.84 \mu\text{m}$  and  $\lambda_p = 10.21 \mu\text{m}$ ) [33], and n-InAs with  $\lambda_p = 8.5 \mu\text{m}$  and  $\lambda_p = 10.1 \mu\text{m}$  [34]. (c) propagation length,  $L_p$ , (d) localization,  $\delta$ , (e) figure of merit,  $\text{Re}(\epsilon)^2 / \text{Im}(\epsilon)$  and (f) figure of merit,  $L_p / \delta$  in comparison with other doped semiconductors.

The dispersion relation for SPPs propagating at the interface between two media with opposite signs of the real parts of the dielectric functions  $\epsilon_m$  and  $\epsilon_d$  (e.g. a highly doped semiconductor and air) is given by

$$k_{spp} = k_0 \sqrt{\frac{\epsilon_m \epsilon_d}{\epsilon_m + \epsilon_d}} \quad (2)$$

where  $k_0 = \frac{\omega}{c}$  and  $c$  is the speed of light [2].

Propagation length of surface plasmons  $L_p$ , is given by

$$L_p = \left( 2 \operatorname{Im} \left[ k_{spp} \right] \right)^{-1}. \quad (3)$$

Localization (confinement factor) in air  $\delta_d$  and in doped semiconductor  $\delta_m$  are given by

$$\delta_{d/m} = \left( 2\pi \sqrt{k_{spp}^2 - \epsilon_{d/m} k_0^2} \right)^{-1}. \quad (4)$$

The total SPP localization is defined as  $\delta_{spp} = \delta_d + \delta_m$ . To compare data reported for different doped semiconductors for mid-IR plasmonics, we plotted in Fig. 3 the complex permittivities, propagation lengths of surface plasmons, its localization, and figures of merit (FOMs). We use two figures of merits defined [35] as

$$\text{FOM}_1 = L_p / \delta_{spp} \quad (5)$$

$$\text{FOM}_2 = \operatorname{Re}(\epsilon)^2 / \operatorname{Im}(\epsilon) \quad (6)$$

in order to quantify the tradeoff between the confinement and propagation loss.

The real part of the doped InP permittivity is more or less comparable with those of other semiconductors [Fig. 3(a)]. It means that InP:Si plasmonic behavior is similar to that of InAs [34] in terms of the value of permittivity and operating wavelength. The imaginary part in turn, is quite low as shown in Fig. 3(b).

From Fig. 3(c), we can see that the SPP propagation length for InP:Si is among the longest for doped semiconductors with  $\lambda_p$  in the 4.47-10.1  $\mu\text{m}$  range, confirming that doped InP exhibits low absorption in this wavelength range. The localization degree is comparable to other doped semiconductors [Fig. 3(d)]. Both FOMs for InP:Si are among the largest for the wavelengths  $\lambda > 10 \mu\text{m}$  thanks to the smaller imaginary part of the permittivity with similar levels of doping [Figs. 3(e) and 3(f)]. If we take into account the position of plasma wavelength  $\lambda_p$ , doped InP exhibits a superior plasmonic performance for the mid-IR regime ( $\lambda > 10 \mu\text{m}$ ) compared to semiconductors with  $\lambda_p$  in the 4.47-8.5  $\mu\text{m}$  range. Even two cases of n-InAs and n-InSb with quite low plasma frequency ( $\lambda_p \approx 10 \mu\text{m}$ ) only partially overperform n-InP in particular parts of the mid-IR spectrum, see FOMs in Figs. 3(e) and 3(f).

### 3. Surface plasmon-polaritons on highly doped InP surface

Since  $k_{spp} > k_0$ , SPPs cannot be excited directly by light beams incident from air, and phase matching techniques for example, prism coupling or grating coupling, are required to provide enough momentum for light to excite SPPs.

To elucidate the excitation of plasmons on the highly doped layer of InP:Si, in the so-called Otto-Kretschmann configuration we employ a high refractive index hemi-spherical germanium prism ( $n_p = 4.0$ ). The reflection spectra in such configuration were theoretically analyzed using the transfer-matrix formalism [36]. In the analyzed configuration, a four-layer



structure of Ge prism/Air gap/InP:Si/InP:S substrate was assumed as illustrated in Fig. 4(a). The Drude-Lorentz model (1) with the sample 1 parameters for the epilayer and its substrate was exploited.

In Fig. 4(b), numerical results are shown for TM-polarized incident light. The dispersion of SPPs on air/InP:Si and InP:Si/InP:S substrate interfaces was calculated by using Eq. (2). These dispersions are also plotted in Fig. 4(b) to give an insight into two kinds of plasmons existing in our system, namely one supported at the air/InP:Si interface (blue diamonds) and another at the InP:Si/InP:S interface (red circles) interface. From the dispersion of a semi-infinite arrangement and the simulation of reflectance, we can deduce that for  $\lambda > 8 \mu\text{m}$  a SPP on the air/InP:Si interface emerges until around  $\lambda = 14 \mu\text{m}$ , and from  $\lambda = 11 \mu\text{m}$  another SPP supported at the InP:Si/InP:S substrate interface appears. Note that the second plasmon mode disappears around  $\lambda = 15 \mu\text{m}$  because the permittivity of the InP substrate also becomes negative at  $\lambda = 16.6 \mu\text{m}$  [Fig. 2(a)] and plasmons at the InP:Si/InP:S interface cannot be supported anymore.

In our experimental setup based on the Otto-Kretschmann configuration [Fig. 4(a)], a hemi-spherical Ge prism was placed on the sample with some air gap between the prism and InP:Si layer. The thickness of the air gap  $d_c = 400\text{nm}$  was evaluated by fitting the experimental results with the simulated reflection spectra. The hemi-spherical Ge prism was adopted for its high refractive index and transparency in the mid-infrared region. A wire-grid polarizer was used in the FTIR setup in order to provide TM-polarized incident light, which was focused on the structure through a parabolic mirror and the Ge prism. Incident light was directed onto the surface with angle of incidence  $\theta_{in}$  which was manually controlled by using a goniometer with the increment of  $2^\circ$ . Series of reflection spectra are joined to form a reflectance map as shown in Fig. 4(c). Note that the critical angle between the Ge prism and air is  $14.47^\circ$ , therefore the simulation and experiment were conducted well above this angle.

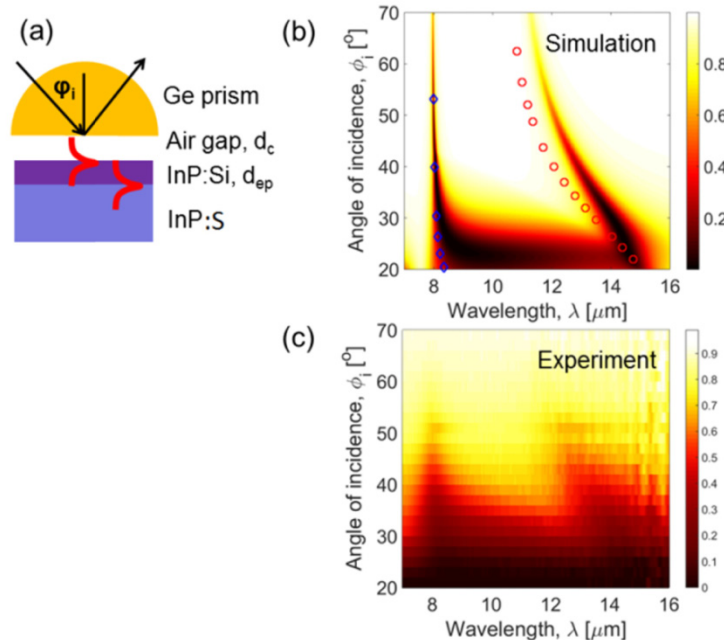


Fig. 4. (a) Illustration of Ge prism/Air gap/InP:Si/InP:S substrate structure with air gap of 400 nm and 400 nm thick InP:Si layer. (b) Simulated and (c) measured reflectance from the structure under consideration. In (b), the dispersion of plasmons supported at the air gap/InP:Si interface (blue diamond) and those at the InP:Si/InP:S substrate interface (red circle) are shown to clarify the origin of two plasmons.

The acquired reflection data as shown in Fig. 4(c) reproduces the theoretical predictions for plasmons on two different interfaces, showing two corresponding reflection bands. All measured reflection dips agree with the theoretical expectations in the wavelength range of  $\lambda = 8 - 15 \mu\text{m}$ . Importantly, the agreement between the observed and theoretical expectations demonstrates that the highly doped InP is an effective plasmonics material for the mid-infrared region, as well as the validity of our fitting method to determine the permittivity of the plasmonic layer. The difference between simulations and experiment in Figs. 4(b) and 4(c) is mainly due to the measurement uncertainties in the FTIR setup including inherent noise of the system, angular uncertainty and polarization mixture at high angles of incidence. Calculation of the beam path in the FTIR setup shows that there is an angular variation of around  $\pm 1.75^\circ$  in the incident light beam which can widen the observed SPP coupling dips in the reflectance spectra. In addition, even though only TM polarized light passes through the polarizer at the input, a small portion of it will be converted to TE polarized light after focusing by the parabolic mirrors of the FTIR reflection accessory. This effect, which is more pronounced at bigger incident angles, will decrease the intensity of the SPP coupling dips in the reflectance spectra.

#### 4. Diffraction of light on highly doped InP grating

Diffraction of light from a periodic grating is governed by Bragg's law

$$k_{out} = mk_g - k_{in}, \quad (7)$$

where  $k_{out} = k_0 \sin \theta_{out}$ ,  $k_{in} = k_0 \sin \theta_{in}$  and  $k_g = \frac{2\pi}{\Lambda}$  are the wave vectors of the diffracted wave, incident wave and grating respectively,  $\Lambda$  is the grating period and  $m$  is the diffraction order. According to the efficiency of the diffraction orders [37] for a grating with a duty cycle of 50% all even diffraction orders must vanish and  $m$  will be an odd integer.

On the other hand, light can couple to a SPP by the grating if the momentum matching condition is satisfied [2]

$$k_{spp} = nk_g + k_{in} \quad (8)$$

As explained above, for a grating with a duty cycle of 50%,  $n$  will also be an odd integer.

The excited SPP wave can reversely be diffracted by the grating into free space, with a wave vector given by

$$k_{out} = mk_g - k_{spp} \quad (9)$$

Applying Eq. (8) in Eq. (9) yields a modified diffraction law [38]

$$k_{out} = (m - n)k_g - k_{in}, \quad (10)$$

where  $m - n$  is now an even integer. This manifests the emerging of even diffraction orders banned by Bragg's law. Such process, when prohibited diffraction orders are facilitated by assistance of SPPs is currently considered as a very promising direction in sensing and new grating functionalities [39,40].

Sample 2 was used to fabricate a diffraction grating with a period of  $50 \mu\text{m}$  and duty cycle of 50%. In this regard a  $\text{SiO}_2$  layer with a thickness of  $187 \text{ nm}$  was deposited on top of the sample using plasma-enhanced chemical vapor deposition (PECVD) and patterned by standard photolithography methods and dry etching, in order to serve as a mask for reactive ion etching (RIE) of the InP. Afterwards,  $2 \mu\text{m}$  of the InP epilayer was etched and the  $\text{SiO}_2$  mask was removed by wet etching in buffered hydrofluoric acid. In this way a  $1 \mu\text{m}$  thick highly doped InP:Si layer was kept under the  $2 \mu\text{m}$  high grating in order to support SPP [Fig. 5].

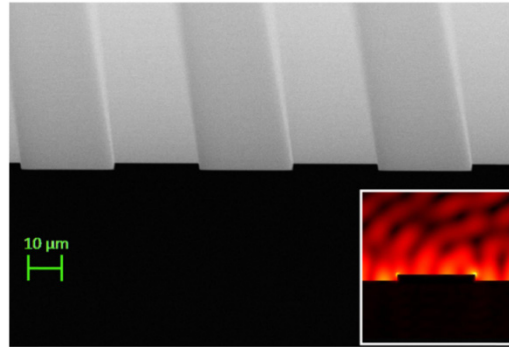


Fig. 5. SEM image of the fabricated grating structure, inset: simulated electric field map for

$$\theta_{in} = 32^\circ.$$

The FTIR setup with a wire grid polarizer was used to measure TM polarized light reflected from the grating. The reflectance was normalized to the reflectance from plain sample 2, and an aperture with 2 mm diameter was used to constrain the angular variation of the focused incident beam. Measurements were repeated three times and then averaged for each incidence angle in order to suppress the noise. Figure 6(a) shows the specular (mode 0) reflectance map where the angle of incidence on the grating is swept from  $14^\circ$  to  $46^\circ$  with an increment of  $2^\circ$ .

The reflectance spectra from the grating were simulated by the finite element method (COMSOL Multiphysics 5.0 [41]) using the Drude-Lorentz dielectric function (1) and parameters found in the previous section for sample 2 and its substrate together with periodic boundary conditions in direction of the periods. The simulated reflection spectrum for each incidence angle  $\theta_m$  is actually the averaged reflection spectra from  $\theta_m - 1.75^\circ$  to  $\theta_m + 1.75^\circ$  with increments of  $0.25^\circ$  in order to imitate the angle uncertainty in the FTIR setup. As it is shown in Fig. 6, the results exhibit good agreement between the simulations and experiment. The dip starting from around  $13 \mu\text{m}$  at  $\theta_{in} = 14^\circ$  and continuing up to around  $17.5 \mu\text{m}$  at  $\theta_m = 46^\circ$  shows the SPP coupling corresponding to  $n = 5$  [Eq. (8)] which is anti-crossed by SPP coupling dips corresponding to  $n = 3$ ,  $n = 2$  and  $n = 1$  at  $13 \mu\text{m}$ ,  $15 \mu\text{m}$  and  $17 \mu\text{m}$  respectively. The dip starting from around  $11 \mu\text{m}$  at  $\theta_{in} = 14^\circ$  and continuing up to around  $13 \mu\text{m}$  at  $\theta_m = 46^\circ$  shows the SPP coupling corresponding to  $n = 6$  [Eq. (8)] which is anti-crossed by SPP coupling dips corresponding to  $n = 3$  and  $n = 2$  at  $11.5 \mu\text{m}$  and  $12 \mu\text{m}$  respectively. SPP coupling dips which happen at lower wavelengths are less pronounced due to the fact that the real part of the permittivity has less contrast with the permittivity of air on these wavelengths.

Figure 7(a) shows the simulated and measured specular reflection spectra for the angle of incidence  $\theta_{in} = 32^\circ$ . According to Eq. (8), at this angle, light couples to a SPP at  $\lambda = 15.45 \mu\text{m}$  for  $n = 5$  and according to Eq. (10), when the incident light couples to the SPP, the previously vanishing mode  $m - n = -2$  emerges as a reflected beam with  $\theta_{out} = 5^\circ$ . Figure 7(b) shows the simulated and measured reflected light at the output angle of  $5^\circ$ , apparently as mode  $-2$ . The slight deviation between the SPP coupling wavelength predicted by Eq. (8) and

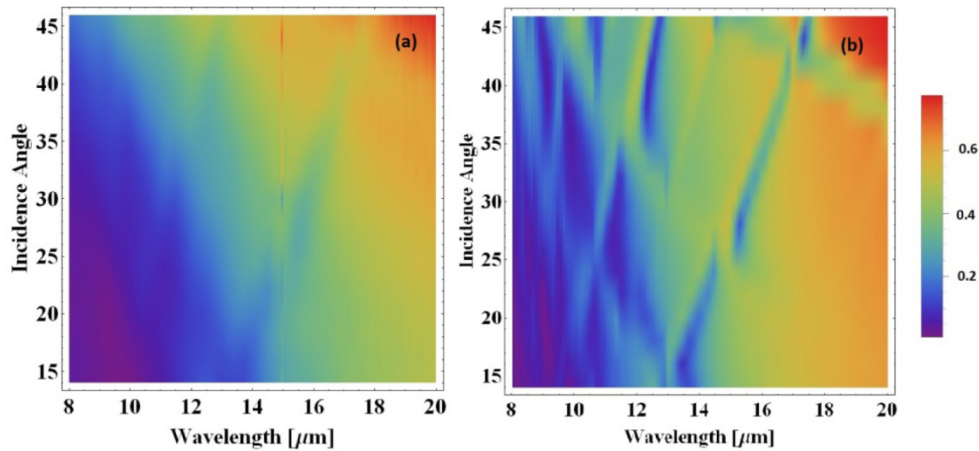


Fig. 6. (a) Experimental and (b) simulated reflectance map from the grating

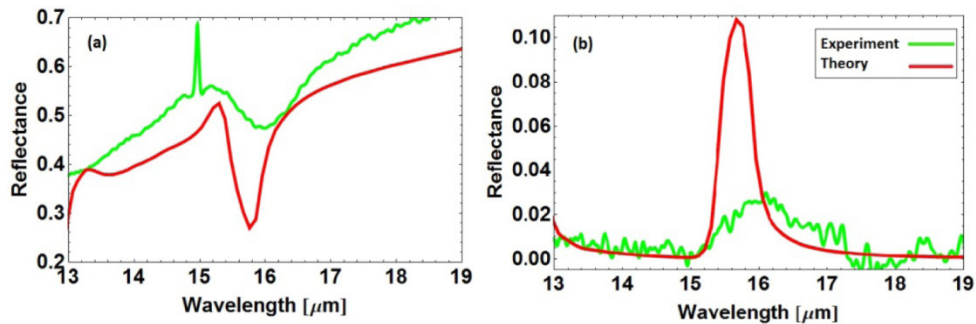


Fig. 7. (a) Mode 0 reflection from the grating.  $\theta_{in} = -\theta_{out} = 32^\circ$  (b) mode  $-2$  reflection from the grating.  $\theta_{in} = 32^\circ$  and  $\theta_{out} = 5^\circ$ .

observed in the simulation and experiment is believed to be mainly due to the uncertainties in the FTIR setup as explained in section 3, namely inherent noise of the system, angular uncertainty and polarization conversion. These uncertainties which are an inseparable part of FTIR diffraction experiments tend to diminish the SPP coupling features in the reflection spectra from the grating as was observed before [40]. This also explains visible deviations in the resonances parameters in simulations and characterization in Figs. 7(a) and 7(b). The sharp peak observed at around  $15 \mu\text{m}$ , also visible as a vertical line in Fig. 6 (a) for all angles is attributed to the measurement system's noise and thus should be ignored.

## 5. Conclusion

In conclusion, we made detailed study of doped InP as a plasmonic material. InP:Si was grown by MOVPE and the growth conditions were optimized to increase the free electron concentration. The Drude-Lorentz dielectric function was used to calculate the reflectance from the grown samples and its parameters were found by fitting the calculated reflectance with the measurement results. It appeared that highly doped InP has a reasonably long propagation length. The figures of merit for InP:Si calculated according to Eqs. (5) and (6) are among the highest for wavelengths over  $10 \mu\text{m}$  due to the small imaginary part of the permittivity for the mid-IR regime. We confirmed experimentally existence of mid-IR surface plasmons at highly doped InP:Si/air and highly doped InP:Si/low doped InP:S interfaces. Measured SPPs dispersion is in a good agreement with simulations based on the fitted

dielectric function. We fabricated an InP:Si grating and characterized diffraction of light in different orders. Appearance of the orders prohibited by the conventional Bragg law manifests the efficient SPPs assistance in light diffraction on plasmonic gratings.

Thus, doped InP can be added to the nomenclature of potential plasmonic materials for the mid-IR regime.

### **Funding**

Support from the Villum Fonden and Ib Henriksens Fond and also partial support from the FP7-PEOPLE-2013-IRSES project HyMeCav (No. 612564) are acknowledged.

### **Acknowledgments**

The authors would like to thank Luisa Ottaviano for her valuable suggestions regarding the fabrication of the grating.